7th US National Technical Meeting
of the Combustion Institute
Hosted by the Georgia Institute of Technology, Atlanta, GA
March 20-23, 2011.

Investigation of Combustion Processes in Miniature Internal Combustion (IC) Engines.

Shyam Menon and Christopher Cadou

Department of Aerospace Engineering, University of Maryland at College Park, College Park, Maryland 20742, USA

Miniature (sub kilogram) glow ignition internal combustion (IC) piston engines are an off–the–shelf technology that could dramatically increase the range and endurance of small unmanned air vehicles provided their overall thermodynamic efficiencies can be increased to 15% or better. Comprehensive measurements of engine losses suggest that incomplete combustion accounts for 60-70% of total energy losses and is the major obstacle to meeting this efficiency goal. A net heat release analysis based on cylinder pressure measurements suggest that a two–stage combustion process occurs at low engine speeds and equivalence ratios close to 1. Different theories based on burning mode and reaction kinetics are proposed to explain these observations. High speed imaging of the combustion chamber suggests that combustion begins in the vicinity of the glow plug in a turbulent premixed mode but that a delayed secondary ignition may occur near the walls. The locations of miniature IC engines on a turbulent combustion regime diagram show that these engines operate in the 'flamelet in eddy' regime whereas conventional–scale engines operate mostly in the 'wrinkled laminar flame sheet' regime.

1. Introduction

Miniature glow ignition internal combustion (IC) engines weighing less than a kilogram have potential to be used as high energy density power sources in various applications. These include propulsion systems for unmanned aerial vehicles (UAV's) as well as replacements for electrochemical power sources in portable applications requiring compact power [1]. Although these engines have existed for 50+ years, their usefulness to these modern applications is limited by a lack of reliable information regarding their fundamental operation and performance characteristics. A multi-year investigation of miniature engines at the University of Maryland has focused on acquiring detailed performance measurements including those for power output and efficiency from a range of engines weighing between 15 g to 500 g [2]. Results have shown that the key to improving current performance levels to meet and exceed power and energy density targets for next generation portable power devices lies in improving the overall conversion efficiency. A detailed experimental investigation undertaken to quantify the sources of energy loss in miniature IC engines identified incomplete combustion loss to be the major factor limiting performance in miniature IC engines [3].

The combustion process occurring in miniature glow ignition IC engines is currently poorly understood. In-cylinder pressure measurements by Dunn-Rankin concluded that combustion occurred in a combination of diesel and partially premixed modes with fuel vapors from the

walls forming a fuel-rich zone next to it resulting in a diffusion driven process [4]. Similar measurements by Raine et al investigated cycle-to-cycle variation in fired cycles of a miniature glow ignition IC engine and attributed the observed variation to the presence of trapped radicals from the previous engine cycle [5]. The most detailed photographic information regarding ignition and combustion phenomena in miniature IC engines is reported by Manente who reported 'dual mode combustion' where the charge sometimes ignited and burned homogeneously and sometimes burned in a premixed flame mode [6].

The work presented here attempts to enhance understanding of the combustion process in miniature IC engines by using a combination of experimental techniques and analytical work to place the combustion process on a combustion regime diagram. The experimental work includes measurements of in-cylinder pressure as well as high speed imaging of the combustion zone during fired engine cycles. Measurements of in-cylinder pressure are used with a single zone heat release model to calculate net heat release rates during the combustion part of the engine cycle. The variation of the location of the engine operating point in the combustion regime diagram is explored as a function of engine size, speed, and equivalence ratio. Taken together, we hope that this information will lead to improved understanding of the turbulent combustion process associated with energy release in miniature IC engines.

2. In-Cylinder Pressure Measurement

In–cylinder pressure comprises a fundamental measurement that describes the instantaneous state of the gas mixture in the cylinder volume during an internal combustion engine cycle. It has been used to study various engine phenomena such as ignition [7], combustion, knock [8] and cycle to cycle variation in conventional scale engines [9]. In the present work, cylinder pressure is measured using a Model M3.5x0.6mm sensor manufactured by Optrand Inc. The sensor operates by measuring the intensity of light reflected from one or more optical fibers placed in front of a flexing metal diaphragm [10]. Crank angle is measured using a rotary shaft encoder.

Engines

Cylinder pressure measurements have been made in three engines: the OS 25 FX, OS 40 FX and the OS 46 FX engines. All engines are manufactured by OS Engines Inc. and are single cylinder, air cooled, glow ignition engines operating on a fuel mixture consisting of methanol, nitromethane and oil. The specifications of the engines are summarized in Table 1.

Engine Model		Displacement		Mass	Geometric compression ratio	Bore	Stroke
A	OS 46 FX	0.46	7.5	488	16.52	22	19.6
B	OS 40 FX	0.4	6.5	386	14.49	20.5	19.6
C	OS 25 FX	0.25	4.1	248	17.96	18	16
		cu. in.	cc	g		mm	mm

Table 1: Specifications of miniature IC engines tested in the study.

Sensor Installation

The sensor is installed in a hole drilled into the stock cylinder head and tapped with the correct thread size. Different numbers of sealing washers between the transducer flange and the head are

used with different engines so as to minimize changes to the dead volume and to ensure that the sensor's diaphragm blends smoothly with the bowl.

Crank angle measurement

The crank angle location corresponding to individual cylinder pressure measurements is made using a Model 260 rotary shaft encoder made by Encoder Products Inc. The encoder is an incremental type quadrature encoder whose output consists of two separate pulse trains as well as an index pulse which can be aligned with any position of the crank shaft. The incremental encoder requires an index pulse and a counter to establish the location of the shaft. The index pulse is provided by the encoder and the counting is done using the data acquisition hardware. A set screw on the shaft encoder allows the rotating part to be locked on to the engine shaft at any location.

Data Acquisition

A National Instruments data acquisition module (NI USB–6221 BNC) was used to measure signals from the cylinder pressure sensor and the outputs of the quadrature encoder. A LABVIEW™ program simultaneously records data from the cylinder pressure sensor and the shaft encoder. During engine operation, the index pulse from the shaft encoder (channel A) is used to trigger the acquisition of cylinder pressure data for each engine cycle. Since the encoder produces 360 pulses per revolution, pressure data is acquired for every degree of crank angle rotation.

Dynamometer Setup

A detailed description of the dynamometer system used to measure miniature engine performance has been presented elsewhere [11]. Therefore, only the modifications associated with cylinder pressure and crank angle measurements are described here. The cylinder pressure sensor is mounted in the cylinder head and the shaft encoder is coupled to the engine shaft. Figure 1 is a photograph of the dynamometer setup for the OS 40 FX engine measurements.

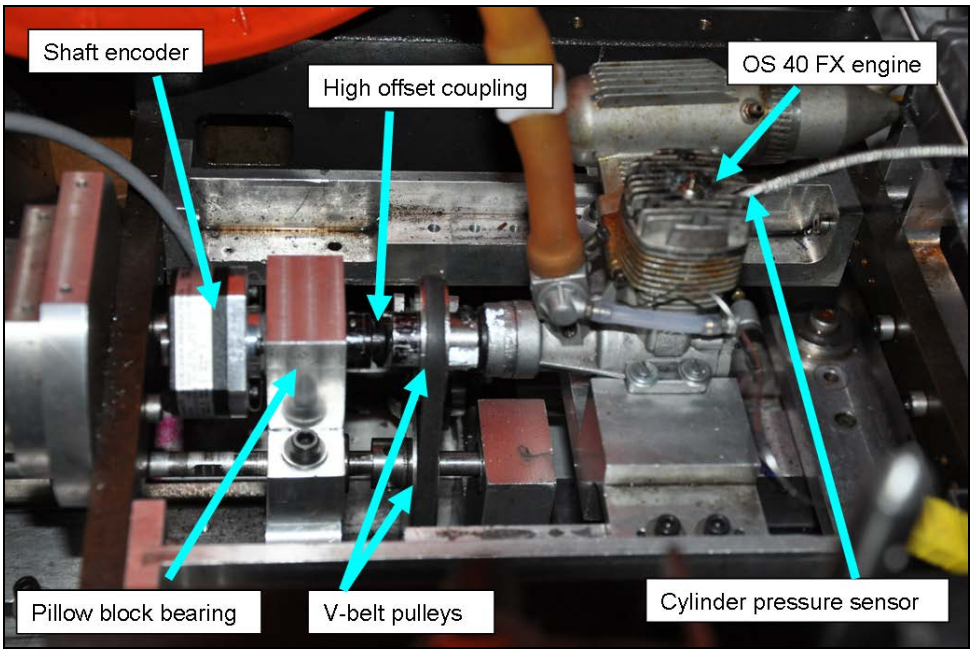

Figure 1: Dynamometer setup for the cylinder pressure measurements on the OS 40 FX engine.

Procedure

The engine is started on the dynamometer using a starter motor and by applying current to the glow plug. All measurements are performed at wide open throttle (WOT). The control system which allows for automated control of engine operating speed is switched on and the desired speed and mixture settings are established. Measurements are obtained from all the sensors on the dynamometer and a similar procedure is repeated for different engine speeds, fuel-air mixture settings and finally for different engines.

Results and Analysis

Cylinder pressure measurements under fired conditions were obtained for three different engines mentioned previously in Table 1. Measurements of power output from the engines were made with and without the cylinder pressure sensor installed. Similar levels of power are obtained in the two cases. This ensures that installation of the sensor produced a minimal change in dead volume and engine compression ratio.

Cylinder Pressure Trace

Figure 2 is a plot of average cylinder pressure as a function of cylinder volume for the OS 25 engine for one operating condition. All pressures reported here are absolute (i.e., sensor output plus ambient pressure). The pressure trace is obtained using an average of 50 engine cycles. The shape of the pressure trace is similar to that observed in conventional–scale two–stroke engines. The compression and expansion parts of the cycle resemble the general form of isentropic curves for the same. The energy release portion of the cycle appears to occur at mostly constant volume as in the idealized Otto cycle. Similar results are obtained for the two other engines tested in this work.

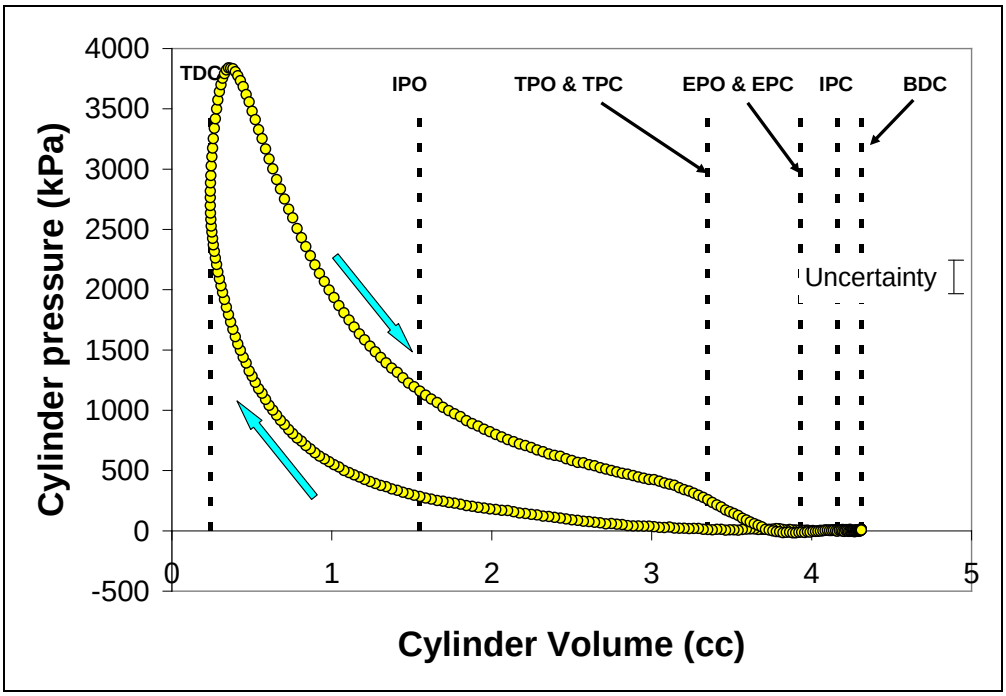

Figure 2: Cylinder pressure plotted as a function of cylinder volume for a fired engine cycle for the OS 25 FX engine operating at a speed of 10000 rpm and an equivalence ratio of 1.05.

Single Zone Model for Net Heat Release Rate

A single zone model of the cylinder volume is used to estimate the heat release rate. The procedure used here is as outlined in Heywood [12]. The final expression for net heat release rate is expressed similar to that in Heywood.

$$\frac{dQ_{\text{net}}}{d\theta} = \left(\frac{C_v}{R} + 1\right) p \frac{dV}{d\theta} + \frac{C_v}{R} V \frac{dp}{d\theta} \tag{1}$$

Equation 1 gives the 'net' heat release rate: ie. the total heat release rate due to combustion minus the heat lost via blowby and heat transfer to the environment. This is the energy that is left to do useful shaft work. This expression is convenient because it is only a function of pressure and therefore can be computed from cylinder pressure measurements.

Figure 3 shows the net heat release rate computed for the OS 25 FX engine operating at a speed of 10000 rpm and an equivalence ratio of 1.05. Heat release rate is computed based on the cylinder pressure trace averaged over 50 cycles. Some amount of scatter is observed in the estimated net heat release rate – particularly before ignition and at about 240 degrees after BDC in the case shown here. The 5 point moving average removes some of the scatter and gives a better picture of engine heat transfer processes [13]. Net heat release rate begins a slow decrease about 100 degrees after BDC and continues to drop until about 160 degrees after BDC. This is presumably due to a combined effect of heat transfer from the gases undergoing compression to the cylinder walls as well as possible blowby from the cylinder to the crankcase. Notice that the heat release rate goes positive near TDC. The point at which net heat release rate goes positive is determined to be the location of start of combustion. Heat release rate peaks at about 200 degrees after BDC. Beyond this point, the heat release rate remains positive but begins to decrease and eventually becomes negative at about 270 degrees after BDC.

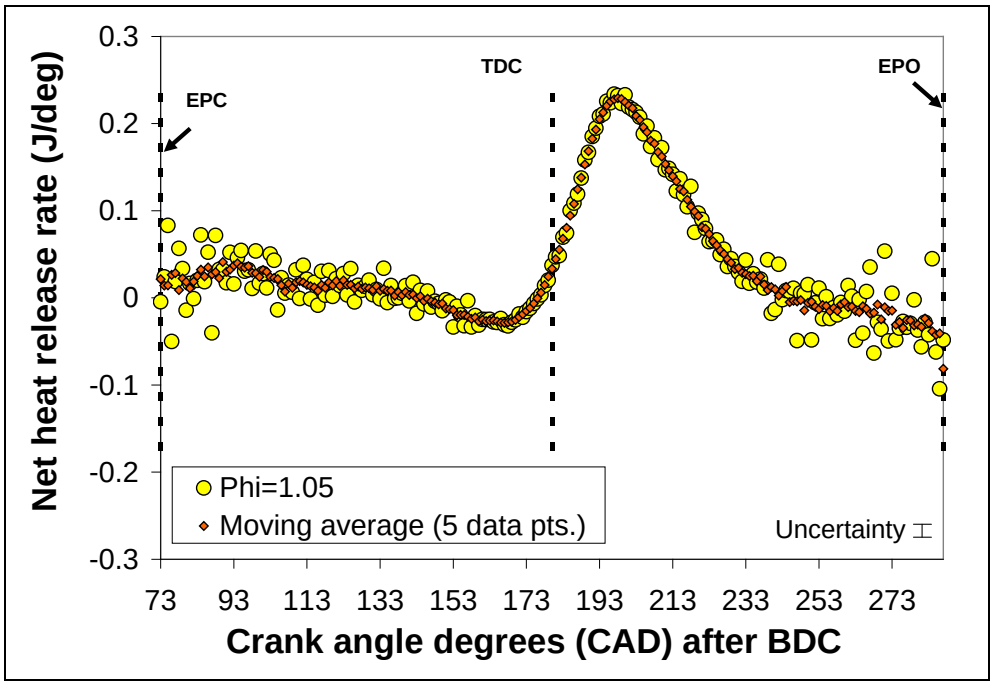

Figure 3: Net heat release rate and a moving average estimated for the same over 5 data points plotted a function of crank angle for the OS 25 FX engine operating 10000 rpm and an equivalence ratio of 1.05.

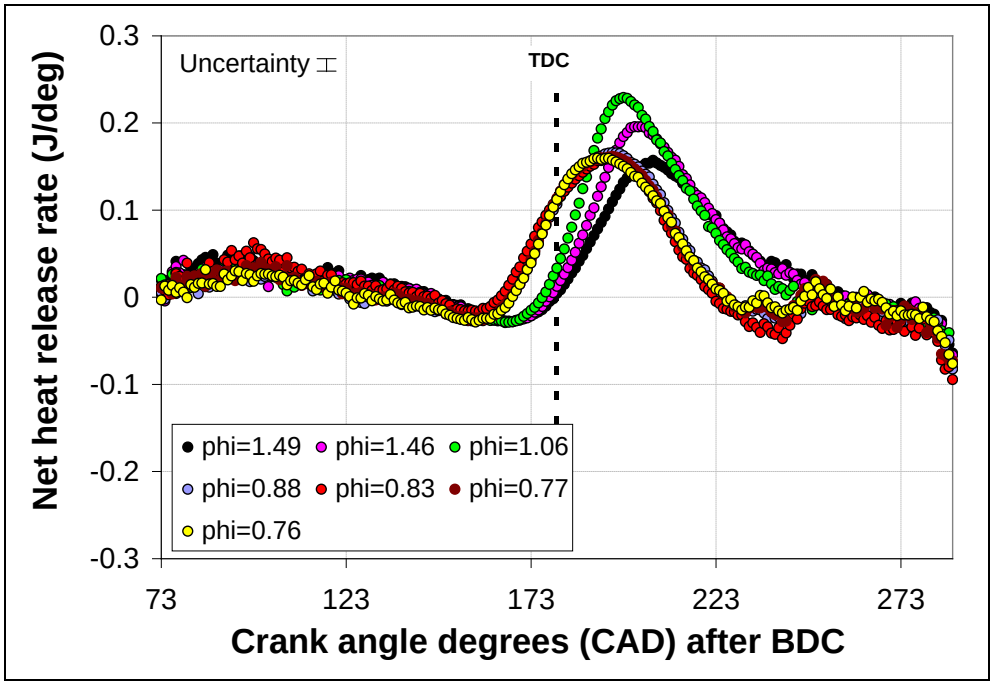

Figure 4: Five point moving average of the net heat release rate estimated for the OS 25 FX engine plotted as a function of crank angle for the engine operating at 10000 rpm and different equivalence ratios.

Figure 4 compares the net 5 point moving averaged heat release rates estimated at 10000 rpm in the OS 25 FX engine for 7 different equivalence ratios. As seen in the figure, the primary effects of changes in equivalence ratio are reflected in the heat release rate during the combustion

portion of the engine cycle. Figure 4 shows that the peak heat release rate occurs slightly rich of stoichiometric.

Figure 5 compares net 5 point moving average heat release rates in the OS 25 FX engine at 7 different speeds and a constant equivalence ratio of about 0.98. The variation in engine speed has a very interesting effect on the net heat release rate. At high engine speeds (10000 and 11000 rpm) the net heat release rate has a single peak similar to those observed in Fig. 4. However, at 9000 rpm and below, the net heat release rate develops a second peak that occurs well before TDC and increases in strength as engine speed decreases.

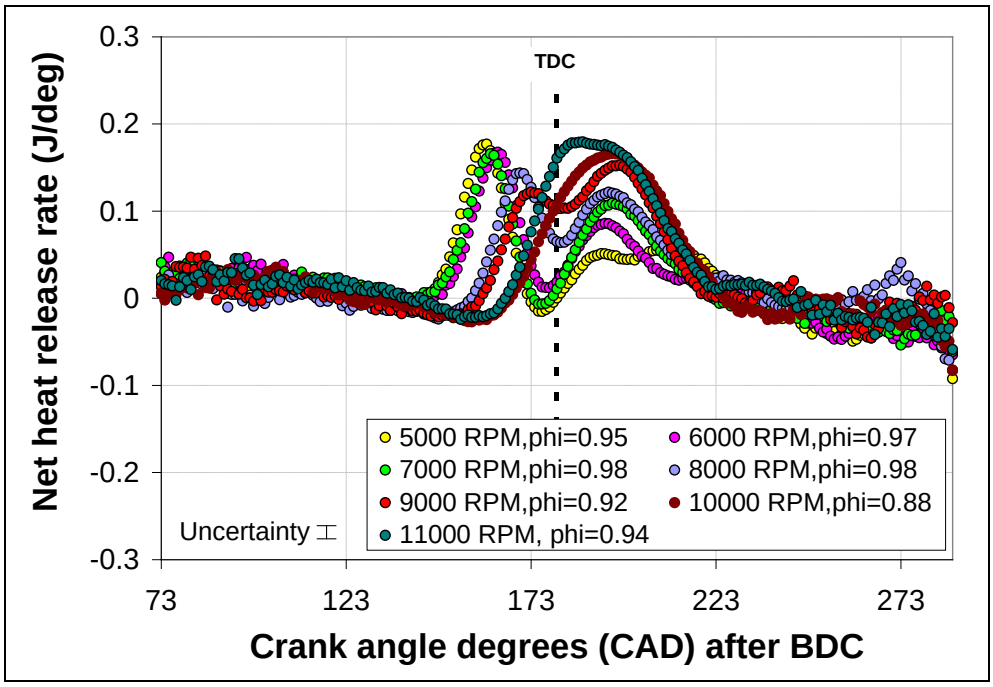

Figure 5: Five point moving point average of the net heat release rate estimated for the OS 25 FX engine plotted as a function of crank angle for the engine operating at different speeds and an equivalence ratio of ~ 0.95.

The heat release rate in these cases decreases sharply between 6 and 19 degrees BTDC after an initial increase and reach a minimum value at around 176 to 185 degrees after BDC. The heat release rate then gradually increases until it reaches a second peak around 191–199 degrees after BDC and starts to drop in a manner similar to that seen earlier in Fig. 4 until the exhaust port opens. This suggests that some type of two–stage combustion process is occurring.

A two–stage combustion process involving a premixed phase and a mixing controlled phase due to fuel injection gives rise to a double peak in net heat release rate in direct injected diesel engines [14]. However, no such fuel injection driven phenomena occurs in miniature glow engines. A similar occurrence in spark ignited engines which are premixed similar to miniature glow engines could not be found in published literature. Hence, only speculative explanations for the double peak phenomena observed with heat release rate can be offered at this point.

One possible explanation is based on a two stage combustion process with the primary ignition and combustion of a premixed charge via turbulent flame propagation followed by diffusion controlled burning of fuel droplets deposited on the cylinder walls. As will be seen in the latter part of this paper, where high speed combustion images are obtained for a larger glow engine

(OS 46 FX), the primary phenomenon driving fuel air combustion appears to be the propagation of a turbulent premixed flame having its origins in the vicinity of the glow plug. However, at lower engine speeds (about 8000 rpm), a secondary burning phenomenon appears to occur near the walls. This observation in conjunction with the observations above suggest that the following possible mechanism for the combustion process: The heat release associated with an initial premixed burning process occurring in the center of the chamber away from the walls vaporizes a liquid fuel film or droplets deposited on the cylinder walls. This fuel diffuses away from the wall into the hot products of the premixed combustion event and eventually ignite. A delay associated with the mixing and ignition time of the secondary process produces the two distinct heat release peaks. Increasing the speed reduces the time available to complete the secondary combustion process resulting in the eventual disappearance of the secondary peak. It also raises the in–cylinder turbulence level which could increase the size of the premixed charge and decrease the size and number of droplets near the walls.

A second explanation for the double peaks observed in heat release rate is based on reaction kinetics. Because ignition starts well before TDC, chain branching reactions are initiated but get suppressed as the piston moves up and the pressure rises. The reactions do not get going again until the pressure starts to fall again after TDC. At low speeds, the reaction can proceed quite far before getting suppressed by the rise in pressure and so the first peak is much larger. As the speed increases, there is less time for the chain branching reactions to get going before they are cut off and the primary peak gets smaller while the secondary peak gets larger. At very high speeds, there isn't time for the chain branching reactions to get going at all and everything occurs after TDC.

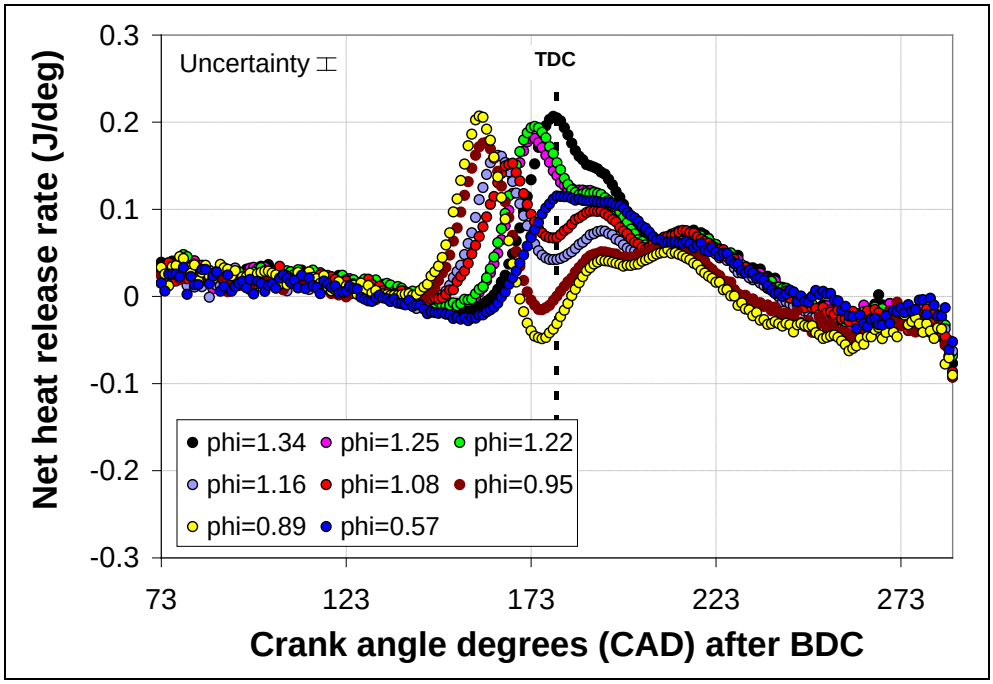

Figure 6: Five point moving point average of the net heat release rate estimated for the OS 25 FX engine plotted as a function of crank angle for the engine operating at 5000 rpm and different equivalence ratios.

Figure 6 shows the net heat release rate as a function of CAD after BDC at 5000 rpm for different equivalence ratios in the OS 25 FX engine. The figure shows that the double peaks

become more apparent when the mixture is close to stoichiometric and are increasingly suppressed as one moves away from stoichiometric conditions. One possible explanation is that the larger heat release per unit charge mass expected at stoichiometric conditions and the larger resulting temperature rise increases the droplet vaporization rate leading to a stronger secondary combustion event. Additionally, the larger heat release could also change the pressure sensitivity of the mixture, making the pressure–sensitive chain branching reactions occur quicker.

Similar double peak behavior was observed in the OS 40 FX and the OS 46 FX engines. However the phenomenon is not as pronounced and appears to get weaker as engine size increases. This suggests that the occurrence of double peaks in net heat release rate is possibly also a scale dependent phenomenon.

3. In-Cylinder Imaging

The in-cylinder imaging work done by Manente described previously required extensive modifications – like relocating the glow plug to near the bottom of the engine cylinder to achieve optical access. These modifications are severe enough that it is unclear how closely the combustion process observed in this engine is related to combustion in the unmodified engine. Therefore, a key goal of the in-cylinder imaging work done here was to provide optical access with as few changes as possible to the physical structure of the engine.

Test Setup

Optical access into the combustion zone is achieved by replacing the stock cylinder head with a quartz disc with a hole at its center to admit the glow plug (OS#8 glow plug with ¼–32 threads) and that has been machined around the hole to duplicate the 'bowl' around the glow plug. The quartz disc is clamped to the cylinder liner using an aluminum ring in exactly the same way as the stock head is clamped to the liner. Optical access is provided through the edges of the disc and through the top of the quartz element via an array of holes bored through the aluminum ring. The original cylinder head bolts are used to sandwich the quartz bowl between the clamping ring and the cylinder liner. The quartz bowl fits directly into a matching recess machined into the bottom surface of the aluminum disk. Figure 7 shows the experimental setup for in–cylinder visualization with the quartz window assembly mounted and secured with cylinder head bolts on the OS 46 FX engine. The engine is held to the test stand using aluminum support blocks and retaining bolts. A nose cone is connected to the propeller to facilitate engine start up. The propeller is for multiple purposes. It applies a load to enable engine speed control, provides cooling air and gives a time reference for the high speed photographs. The photographs are captured using a v12.1 high speed Phantom camera made by Vision Research Inc. In addition to acquiring in-cylinder images, measurements of fuel-air mixture ratio, engine speed, cylinder head and exhaust gas temperatures were also obtained.

Procedure

The camera is positioned in the right location to capture images through the quartz window as well as to view the blade of the propeller cutting across the field of view. The engine is started using a starter motor pressed to the nose cone. The engine is adjusted to the required operating speed and fuel-air mixture setting. The camera is triggered using the control software and a movie is recorded. Simultaneously, measurements are obtained from the flow, speed and temperature sensors using the LABVIEW™ data acquisition setup.

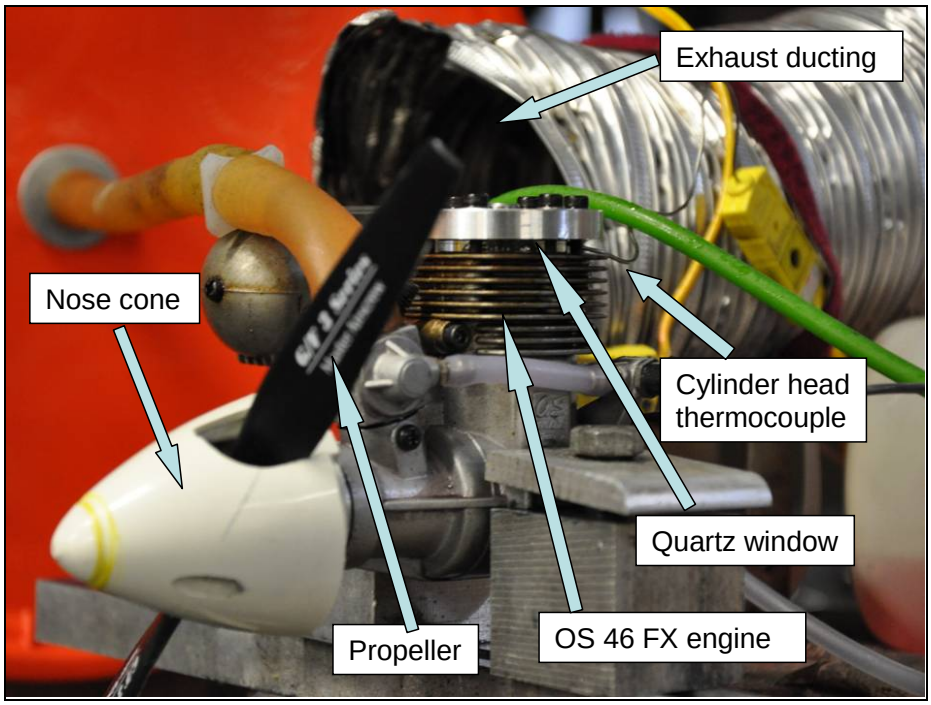

Figure 7: Photograph of the engine test setup on a stand with nose cone and propeller for engine loading.

Results and Analysis

Figure 8 is a false color image of natural luminescence occurring from the combustion chamber for one cycle of the OS–46FX engine operating at a speed of 8000 rpm and a fuel–air mixture ratio of 0.21 or an equivalence ratio of about 1. The corresponding crank angles at approximately 10 CAD intervals are shown in the upper left hand corner of each image and the white lines show the approximate edges of the combustion chamber bowl. The exhaust port is located to the left of the bowl center. The bright spot in the center of the images that remains illuminated throughout the engine cycle is the glow plug. The images from the cycle which show an increase in background luminescence that spreads throughout the chamber beginning at about 100 and ending at about 180 CAD suggests that the combustion event occurs within this interval. The images suggest that the mixture to the left of the glow plug ignites first and a flame front propagates outwards. (See 93.4 – 112.8 CAD in Fig. 8).

Since the images are purely of the light emitted by radiation from soot particles, there is no way to infer the location of the flame from the images. This makes it difficult to infer whether the combustion is characteristic of a premixed turbulent flame or of an HCCI type event. However, the gradual spread of combustion from the exhaust port throughout the bowl indicates a propagation type of phenomenon (possibly initiated by hot products near the exhaust port that are left over from the previous cycle) which is more typical of a premixed flame than that of HCCI combustion. Figure 9 shows the high speed images of the combustion events during another cycle of the OS 46 FX engine operating at 8000 rpm and a fuel–air mixture ratio of 0.21. The figure illustrates several types of irregularities observed in the combustion process in some engine cycles. A soot particle or combustion of a fuel droplet is visible to the left of the glow plug from 122.6 ATDC to 151.8 ATDC and appears to travel some distance across the face of the bowl to the left. Other isolated areas of luminosity at different locations in the cylinder

volume suggest that combustion does not always occur via a propagating flame front. For example, a re–ignition event seems to begin in the lower left of the image at 151.8 ATDC and this could possibly be evidence for the secondary combustion events observed in the pressure measurements reported in the previous section.

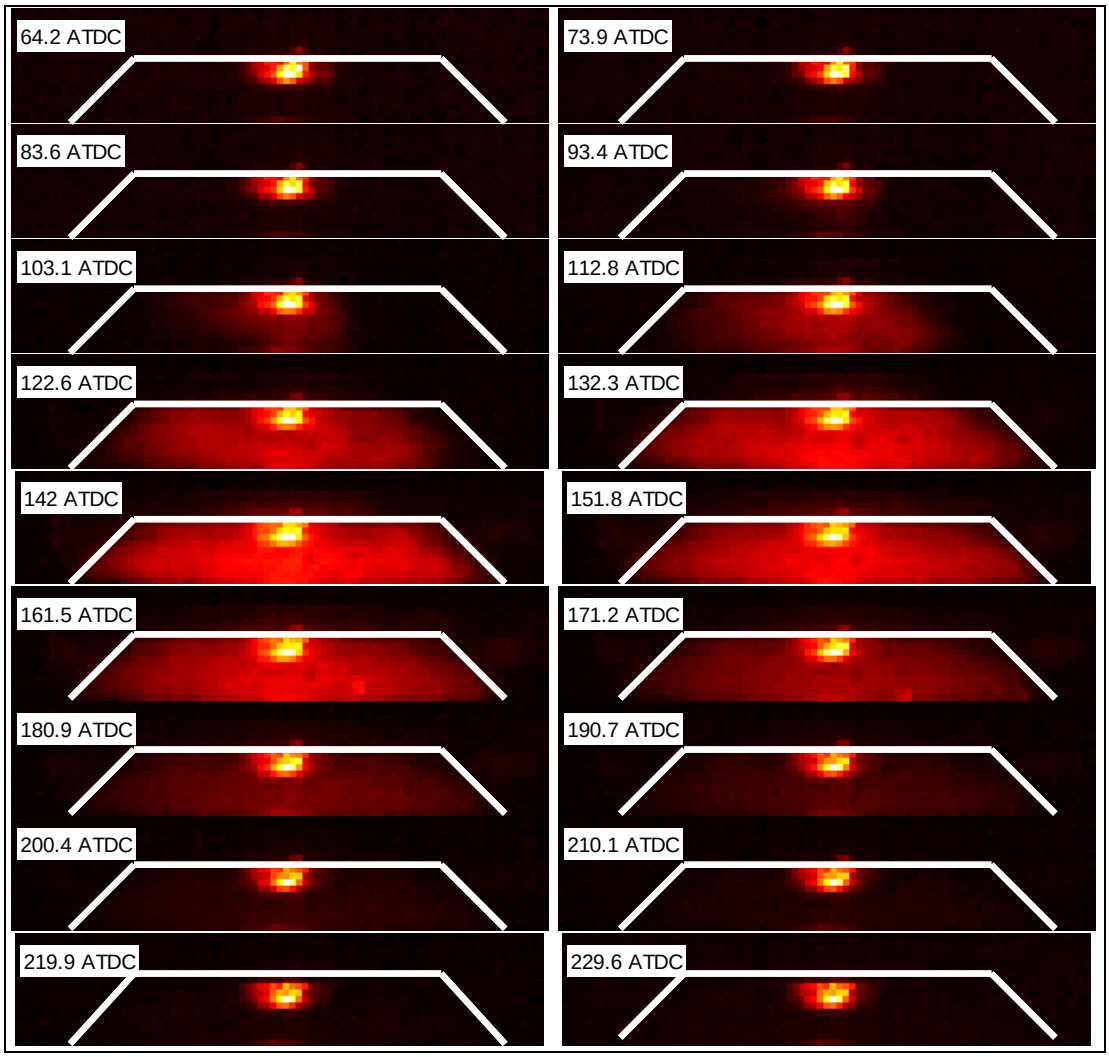

Figure 8: High speed false color images of a single engine cycle during the combustion phase in the OS 46 FX engine at 8000 rpm and a fuel air mixture ratio of 0.21. Uncertainty in crank angle location is about 40 degrees CAD.

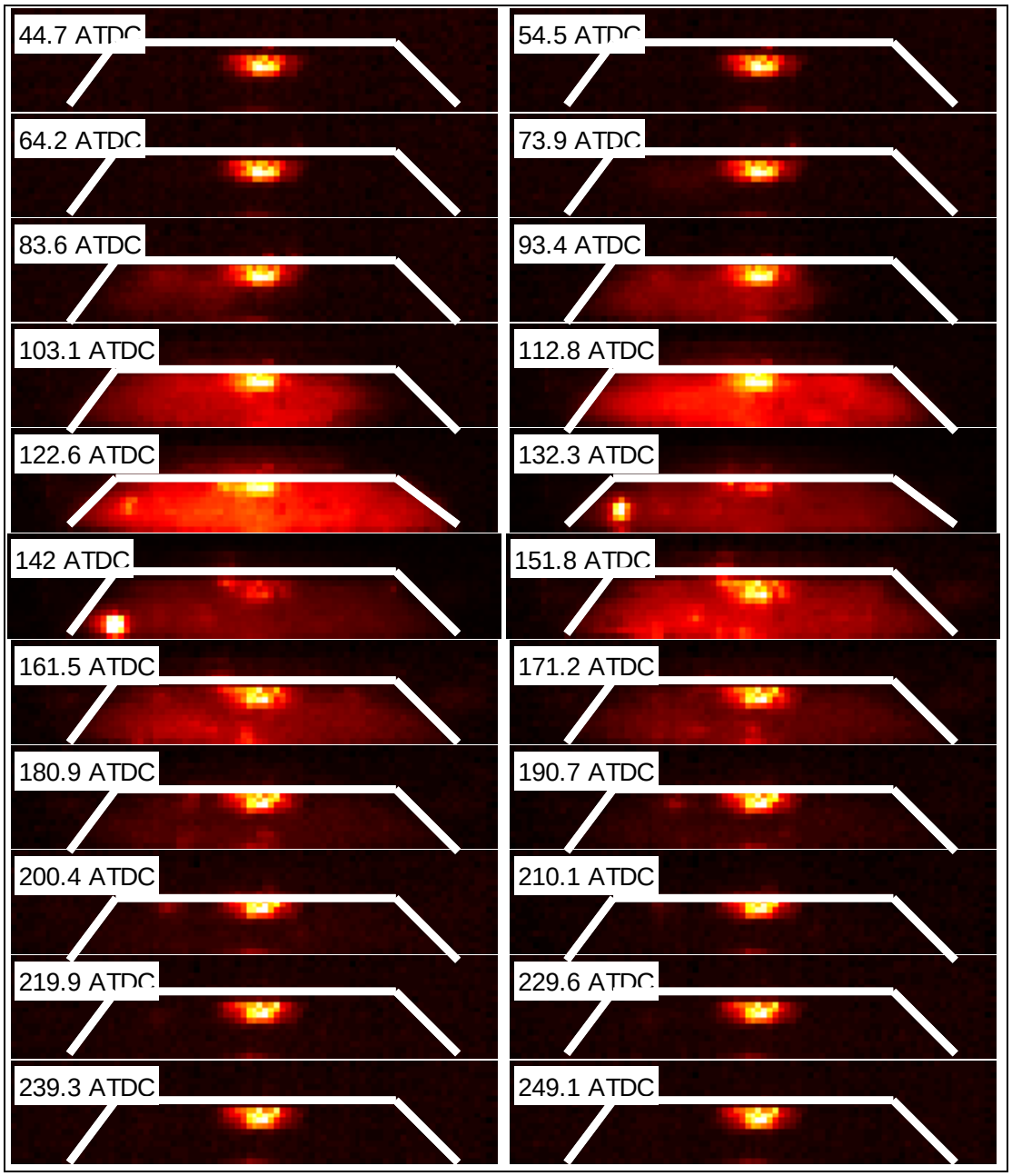

Figure 9: High speed false color images of a single engine cycle during the combustion phase in the OS 46 FX engine at 8000 rpm and a fuel air mixture ratio of 0.21 showing the formation of soot as well as evidence of a thin films of fuel burning on the walls of the quartz window. Uncertainty in crank angle location is about 40 degrees CAD.

4. Combustion Regime Analysis

Abraham and Williams [15] showed that combustion in conventional–scale gasoline and diesel engines generally occurs in a wrinkled laminar flame regime and this has driven the development of IC engine combustion models [16, 17]. The combustion regime associated with miniature engines is not known but is probably different than that occurring in conventional–scale engines for the following reasons:

- Engine operating speeds are considerably higher and engine dimensions are almost an order of magnitude smaller than conventional–scale engines leading to increased importance of wall interactions.
- Crankcase scavenged two–stroke operation potentially results in much greater charge dilution by combustion products.
- Most of these small engines operate considerably rich of stoichiometric [18].

The objective here is hence, to identify the combustion regime associated with miniature engine operation as a first step toward developing a fundamental understanding of combustion in miniature engines and toward developing appropriate modeling strategies.

Regime Diagrams

A regime diagram is a non–dimensional representation of how the ratios of various flow length scales – including the ratio of turbulence length scale to reaction zone thickness – depend on two fundamental dimensionless parameters: the Turbulence Reynolds number and the Damköhler number. Figure 10 is an example that was regenerated based on the work of Abraham et. al. The horizontal and vertical axes are the turbulent Reynolds number and Damköhler number $\frac{v'_{rms}}{S_L}$, $\frac{l_k}{\delta_L}$ and $\frac{l_0}{\delta_L}$ respectively. The solid lines marked on the chart are contours of constant . These ratios show how turbulence rates and turbulence length scales relate to flame speed and flame thickness. The lines delineate the different regimes of turbulent combustion as represented by flamesheets, flamelet in eddy and distributed reactions. A more detailed explanation of the chart can be found elsewhere [19]. The square symbols on Fig. 10 correspond to Abraham et. al's predictions for where various gasoline and diesel IC engines are located in the space while the box shows Abraham et al.'s prediction for where most IC engine combustion processes would lie. Note that while the box spans the flamelet and flame sheet regimes, most of it lies in the flame sheet regime.

Procedure for Placing Engines on the Regime Diagram

Placing engines on the regime diagram requires estimating the Damköhler and Reynolds number at a variety of operating conditions. This, in turn, requires carefully quantifying the range of conditions possible in the engine and determining the laminar flame speed and thickness at each condition. The procedure used here to estimate the Damköhler number and turbulence Reynolds number in different engines is presented in detail elsewhere [20]. This procedure is 'checked' by applying it to the same engines investigated by Abraham et. al. [21] The Damköhler and Reynolds numbers calculated for these engines using the methodology described above are shown by the round symbols in Fig. 10. The fact that they coincide with Abraham's results indicates that applying the procedure outlined above to conventional–scale engines gives results that are consistent with those of other researchers. Now that we have a validated tool, the next step is to apply it to the small glow–fueled engines of interest in this work.

Five different parameters are chosen as variables and the effect of each on the location of the engines in the combustion regime diagram is analyzed using the procedure outlined previously. Table 2 gives the ranges over which each parameter was varied. The 'baseline value' of a parameter is the constant value assigned to it while one of the other parameters is varied. The ranges are assigned based on the range of small engine operating conditions observed in the considerable amount of test data accumulated on the dynamometer device. The fuel is assumed to be methanol in all cases.

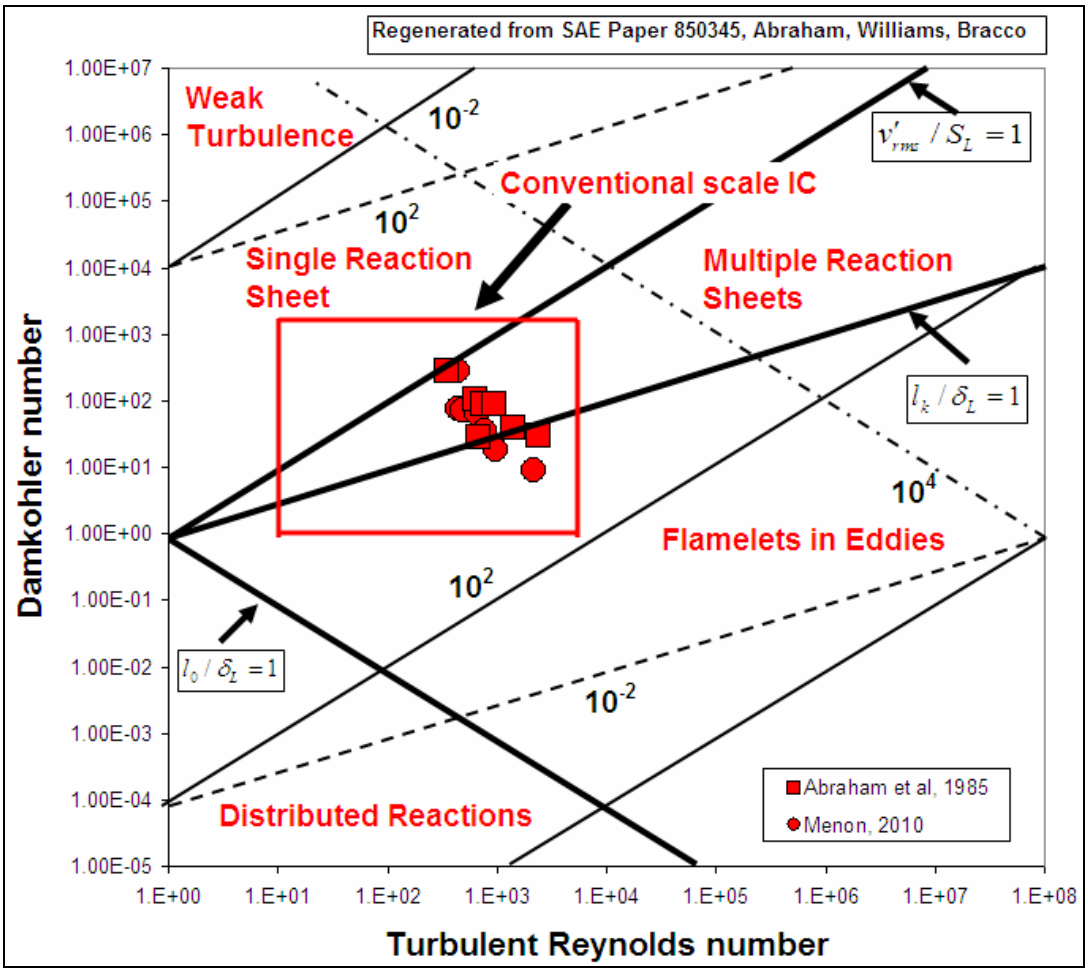

Figure 10: Operating points for internal combustion engines on the combustion regime diagram.

Variable parameter	Range explored	Baseline value	Units
Displacement	0.16–7.54	N/A	cc
Equivalence ratio	0.6–1.6	1	
Speed	5000–15000	10000	rpm
Ignition timing	10 BTDC–5 ATDC	5 BTDC	CAD
Charge dilution	0–45	45	%

Table 2: Variable parameters explored in the analysis of combustion regimes for methanol fueled two–stroke miniature IC engines.

Figure 11 illustrates the effect of various parameters as listed in table 2 on the location of the engine operating point in the regime diagram. The effect of decreasing engine size in all cases is seen to result in shifting the operating point to the lower left of the figure. This is due to the decrease in length scale resulting in a corresponding decrease in both the Damköhler and the turbulent Reynolds number. The effect of changing other variables within the size limits of the

engines explored here, are indicated by the corresponding colored boxes. The effects of these parameters are explained in further detail below.

Effect of Equivalence Ratio

The effect of operating off stoichiometric on the rich or lean side moves shifts the engine down in the regime diagram and can be dramatic for very rich or lean mixtures as it can drive the engine well into the distributed reaction zone regime. This shift is primarily due to the drastic decrease in flame speed as the equivalence ratio is moved away from stoichiometric. The decrease in flame speed results in a consequent decrease in Damköhler number due to longer chemical reaction time.

Effect of Engine Size and Engine Speed

The principal effect of increasing engine speed is to increase the mean piston speed thereby increasing the turbulence intensity. This, in turn, increases the turbulent Reynolds number and decreases the Damköhler number. The net effect of increasing speed is to shift the location of the engines in the regime diagram lower and to the right in the figure. However, the effect of speed is not as strong as that of equivalence ratio. While the combustion regime lies outside the range associated with conventional–scale engines, realistic changes in speed will not drive it out of the flamelet in eddies regime.

Effect of Engine Size and Ignition Timing

Retarding ignition timing from the baseline value of 5 degrees BTDC increases the pressure and temperature at the point of ignition. This increases the flame speed resulting in an increase in Damköhler number without any change in the turbulent Reynolds number. Thus, the location of the engines in the regime diagram shifts upward by a small amount and the combustion mode remains in the flamelet in eddies regime.

Effect of Engine Size and Charge Dilution

The primary effect of increasing charge dilution is to reduce the laminar flame speed. For a charge dilution value of greater than 45%, the flame speed is negative. The decrease in flame speed contributes to a decrease in Damköhler number with no change in the turbulent Reynolds number. The net effect is shift the location of the engines on the regime diagram downward while still occupying the flamelet in eddies regime but tending towards the distributed reaction regime. Changing the in charge dilution seems to have the strongest effect on the location of the engines in the regime diagram after the effect of change in equivalence ratio. Finally, it should be noted that while the baseline charge dilution of 45% puts the baseline engine well outside the regime associated with conventional–scale engines, reducing the dilution to 0% as in a conventional 4–stroke engine puts small engines in the same general combustion regime as conventional–scale engines.

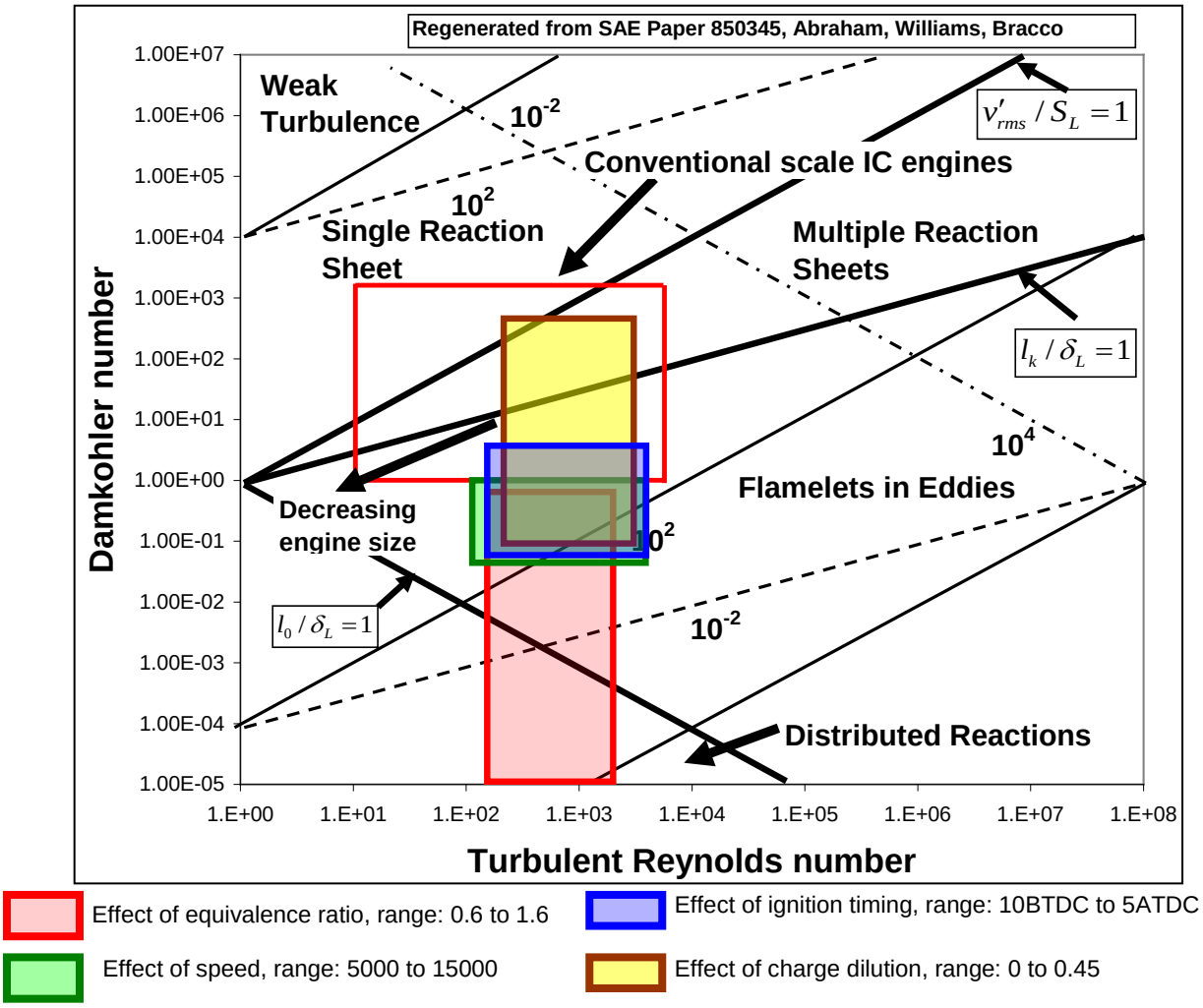

Figure 11: Operating points for methanol fueled two–stroke miniature internal combustion engines showing the effect of variation in engine size and equivalence ratio.

5. Concluding Remarks

In-cylinder pressure measurements made in three different size miniature engines are used to obtain a general understanding of the combustion process and how it is affected by scale. The key findings are that the combustion mode appears to be scale-dependent and that miniature engines may operate in a new regime that will require different combustion models. Equivalence ratio and engine speed are the most important parameters governing peak cylinder pressure and peak engine performance. Peak cylinder pressure and heat release rate decrease as speed increases and equivalence ratio deviates from 1. In smaller engines and at low speed, there is evidence suggesting that a two–stage combustion process occurs. It begins with localized ignition in the region around the glow plug and is followed by a delayed secondary ignition. Evidence of this behavior disappears in all engines as speed increases or fuel to air ratio deviates from stoichiometric suggesting that this is less influenced by scale than the local Damköhler number. One possible explanation of this apparent re–ignition is that radiation from a turbulent combustion process initiated at the glow plug ignites residual fuel near the walls after a delay. Another possible explanation is that this is an artifact of the combustion kinetics in which rising

pressure suppresses chain branching reactions which re–start once the pressure starts to decrease after the piston passes TDC. In either case, this suggests that a major source of inefficiency could be the loss of un-reacted fuel. High speed images of the reacting flow suggest that energy release occurs primarily due to a flame propagation phenomenon however there also is some evidence for a secondary combustion that occurs in a diffusion controlled manner. A regime diagram analysis shows that miniature piston engines operate entirely in the 'flamelet in eddy' regime whereas conventional–scale piston engines span the 'wrinkled laminar flamesheet' and 'flamelet in eddy' regimes but lie mostly in the flame sheet regime. Reducing engine scale drives the combustion regime even closer to distributed reaction. Therefore, it is clear that the approaches used to model combustion in conventional–scale engines are not appropriate for use in miniature engines and different approaches will need to be developed.

Acknowledgments

The authors would like to thank the Army Research Office for supporting this work through the MAV MURI Program (Grant No. ARMY-W911NF0410176), Technical Monitor Dr. Thomas Doligalski.

References

[1] Dunn-Rankin, D., Leal, E.M., and Walther, D., "Personal Power Systems", Progress in Energy and Combustion Science, Vol. 31, Issues 5-6, 2005, pp. 422-465.
[2] Menon, S., Cadou, C., "Investigation of Performance Scaling in Small Internal Combustion Engines", Eastern States Meeting of the Combustion Institute, College Park, MD, 2009.
[3] Menon, S., "The Scaling of Performance and Losses in Miniature Internal Combustion Engines", PhD. Thesis, 2010.
[4] Papac, J. and Dunn-Rankin, D., "Characteristics of Combustion in a Miniature Four-Stroke Engine", Journal of aeronautics, astronautics and aviation Series A, Vol. 38, 2006, pp. 77-88.
[5] Ball, J.K., Raine, R.R., and Stone, C.R., "Combustion Analysis and Cycle-By-Cycle Variations in Spark Ignition Engine Combustion Part 1: An Evaluation of Combustion Analysis Routines by Reference to Model Data", Proceedings of the Institution of Mechanical Engineers, Part D: Journal of Automobile Engineering, Vol. 212, No. 5, 1998, pp. 381-399.
[6] Manente, V., "Characterization of Glow Plug and HCCI Combustion Processes in a Small Volume at High Engine Speed", Phd thesis, Lund University, Sweden, 2007.
[7] Rousseau, S., Lemoult, B., and Tazerout, M., "Combustion Characterization of Natural Gas in a Lean Burn Spark-Ignition Engine", Proceedings of the Institution of Mechanical Engineers, Part D: Journal of Automobile Engineering, Vol. 213, No. 5, 1999, pp. 481-489.
[8] Brunt. M., Pond, C., and Biundo, J., "Gasoline Engine Knock Analysis Using Cylinder Pressure Data", SAE Paper Number: 980896, 1998.
[9] Zervas,E., "Correlations between Cycle-To-Cycle Variations and Combustion Parameters of a Spark Ignition Engine", Applied Thermal Engineering, Vol. 24, Issues 14-15, October 2004, pp. 2073-2081.
[10] Wlodarczyk , M., "Long-Life Fiber-Optic Pressure Sensors for Reciprocating Machinery Monitoring", 9th Trade Fair and Conference Sensor, May 1999, Nuremberg, Germany.
[11] Menon, S., Moulton, N. and Cadou, C. P., "Development of a Dynamometer for Measuring Small Internal-Combustion Engine Performance", AIAA Journal of Propulsion and Power, Vol.23, No.1, Jan-Feb 2007.
[12] Heywood, J. B., "Internal Combustion Engine Fundamentals", McGraw-Hill Book Company, 1988, pp. 386.
[13] Lakshminarayanan, P.A., Aghav, Y.V., Dani, A.D. and Mehta P.S., "Accurate Prediction of the Rate of Heat Release in a Modern Direct Injection Diesel Engine", Proceedings of the institution of mechanical engineers, part D: Journal of automobile engineering, Vol.216, No.8, 2002, pp. 663-675.
[14] Jindal, S., Nandwana, B.P., and Rathore, N.S., "Comparative Evaluation of Combustion, Performance, and Emissions of Jatropha Methyl Ester and Karanj Methyl Ester in a Direct Injection Diesel Engine". Energy Fuels, 2010, Vol. 24, No. 3, pp. 1565–1572.
[15] Abraham, J., Williams, F.A., and Bracco, F.V., "A Discussion of Turbulent Flame Structures in Premixed Charges", SAE paper 850345, 1985.

[16] Cheng, W.K., and Diringer, J.A., "Numerical Modeling of SI Engine Combustion with a Flame Sheet Model", SAE, Paper No. 910268, 1991.
[17] Verhelst, S., and Shepperd, C.G.W., "Multi-Zone Thermodynamic Modelling of Spark-Ignition Engine Combustion – An Overview", Energy Conversion and Management, Vol.50, Iss.5, May 2009, pp. 1326-1335.
[18] Menon, S., Moulton, N. and Cadou, C. P., "Development of a Dynamometer for Measuring Small Internal-Combustion Engine Performance", AIAA Journal of Propulsion and Power, Vol.23, No.1, Jan-Feb 2007.
[19] Turns, S., "An Introduction to Combustion", McGraw-Hill Book Company, Second Edition, 2000, pp. 458.
[20] Menon, S., "The Scaling of Performance and Losses in Miniature Internal Combustion Engines", PhD. Thesis, 2010.
[21] Abraham, J., Williams, F.A., and Bracco, F.V., "A Discussion of Turbulent Flame Structures in Premixed Charges", SAE paper 850345, 1985.